9^{th} *International Conference on* HYDROELASTICITY IN MARINE TECHNOLOGY
Rome, Italy, July 10^{th}-13^{th} *2022*

Estimation of VIV-parameters based on Response Measurements and Bayesian Machine Learning Algorithms

Andersen, M. L.[1*], Sævik, S.[1], Leira, B.[1], Wu, J.[3], Langseth, H.[2],
Yin, D.[3], Lie, H.[3], Passano, E.[3]

[1] Dept. Marine Tech., NTNU, Trondheim, Norway
[2] SINTEF Ocean, Trondheim, Norway
[3] Dept. Computer Science, NTNU, Trondheim, Norway

Abstract. Analysis of structural response levels due to hydro-elastic vortex-induced vibrations (VIV) involves the specification of several parameters both associated with the fluid flow and the structural properties. To the maximum possible extent, the applied values of these parameters should be based on relevant results from experiments and full-scale measurements. This can be achieved by establishing a probabilistic framework which allows continuous learning in relation to the numerical models and associated parameters that are to be applied for the analysis. In this paper, a Bayesian optimization framework for estimating parameters in the VIV time-domain model (VIVANA-TD) is presented. As a case scenario, a simplified VIV model was studied for the purpose of illustration. A simple numerical model of a cylinder with 1 degree of freedom (DOF) was applied in predicting of the time-varying dynamic response. This prediction model is based on the hybrid-analytical concept, which relies on a combination of the time domain model and measured response features. In addition, two methods for estimating the parameter uncertainties are introduced.

Key words: *VIV; Machine learning; Bayesian optimization; Digital twins; Marine risers*

1. Introduction

In marine industry applications concerning long slender structures, such as risers, power cables and mooring lines, fatigue damage related to vortex-induced vibrations (VIV) is a common issue [1]. VIV is a non-linear response type where the structure interacts with the vortices generated in its wake [2]. According to the non-linear nature of the forces and the unpredictability in the response, it is obliged to use high safety factors in engineering concerning VIV [3]. However, by improving the VIV prediction models, the risk of failure can be reduced, leading to lower cost, longer life time and a reduction in materials for future installations.

Prediction models for VIV could in principle be found by solving the Navier-Stokes equations numerically in a computational fluid dynamics (CFD) program, but due to the computational cost of these methods this is not yet feasible. Less costly engineering tools, such as semi-empirical models, have been developed to predict VIV where the structure may be modeled by the finite element method (FEM) and the external forces described by coefficients which are based on experimental results [4]. Among these models are Shear7 [5], VIVA [6] and VIVANA [7], which all are expressed in the frequency domain and applies modal analysis and super position principles to estimate the VIV response along the structure. However, these models do not account for time-varying flow, variable tension or contact interactions between seabed and vessel. Models expressed in the time-domain have later been developed to overcome these problems. One of these models was proposed for cross-flow (CF) vibrations by Thorsen (2014) [8]

[*]Correspondence to: hyel.2022@inm.cnr.it

and has later been improved to model pure in-line (IL) response [9] and combined IL and CF response [10]. The force term in the time-domain VIV is based on the Morison's equation including extra terms to describe the vortex shedding forces, where the synchronization is controlled by a Kuramoto model [11]. The time-domain VIV model has been integrated in the FEM program RIFLEX [12], referred to as VIVANA-TD [13], where the force model includes higher harmonics load terms [14] and new combinations of the CF and IL synchronization terms [15]. The model has been validated with respect to experiments and has in general showed good agreement in predicting fatigue [16]. VIVANA-TD does, however, contain a number of hydrodynamic parameters that need to be estimated.

Yin et al. [17] did an optimization study of the hydrodynamic parameters, applying gradient based methods to minimize the difference in maximum fatigue damage prediction between simulation and experiment. Their results documented good agreement in fatigue life, however, their method did not include uncertainty estimation of the parameters.

Parameter tuning using Bayesian updating methods are often applied as an active learning approach. Han (2021) [18] used discrete Bayesian inference to tune unknown hydrodynamic vessel parameters based on the difference between measured and simulated response amplitudes. Meng et al. [19] presented a multi-fidelity framework for predicting VIV response of a riser. Bayesian inference was used to quantify the uncertainties of response predictions and enabled active learning to improve predictions and reduce uncertainty.

Bayesian optimization [20] is a method that sequentially updates a model by adding new observations in order to optimize a function. The method has shown promising results both when tuning hyper parameters in data-driven (black-box) models but also in case of updating physical parameters in hybrid (grey-box) models [21].

In this paper, a Bayesian optimization framework is proposed to estimate the hydrodynamic parameters in the VIV time-domain model. This was done by sequentially comparing the response from simulations to synthetic data and actively learning the parameters that give the smallest error between the two. In addition, the uncertainty of the parameters was estimated by two different measures. The optimization method was applied to the CF response of a simple rigid cylinder with one degree of freedom (DOF). Both one and two parameter optimization were investigated. The aim is to extend the study by including combined CF and IL response, optimize several parameters simultaneously and finally to use data from model tests to update the parameters.

2. VIV force model

The time domain VIV model (VIVANA-TD) including the semi-empirical force term is at this stage defined for both IL and CF vibrations in [15]. The unit vectors ($\mathbf{j}_1$, $\mathbf{j}_2$, $\mathbf{j}_3$) are defined in Fig. 1. In this paper, a simplified force model concerning only CF excitation is considered:

$$\boldsymbol{F} = \underbrace{C_M \rho \frac{\pi D^2}{4} \dot{\boldsymbol{u}}_n}_{\text{Froude-Krylov force}} \underbrace{- (C_M - 1) \rho \frac{\pi D^2}{4} \ddot{\boldsymbol{x}}_n}_{\text{Added mass force}} + \underbrace{\frac{1}{2} \rho D C_D |\boldsymbol{v}_n| \boldsymbol{v}_n}_{\text{Drag force}} + \underbrace{\frac{1}{2} \rho D C_V |\boldsymbol{v}_n| (\mathbf{j}_3 \times \boldsymbol{v}_n) \cos \phi_{\text{exc}}}_{\text{Cross-flow VIV force}}, \quad (1)$$

where:
ρ: Fluid density
D: Cylinder diameter
$\boldsymbol{u}_n$: Normal component of current velocity in the
$\boldsymbol{x}_n$: Structural displacement in $\mathbf{j}_1\mathbf{j}_2$-plane
C_M: Inertia coefficient, $C_M = 2$ for a circular cylinder
C_D: Drag coefficient
C_V: CF vortex shedding force coefficient
$\phi_{\text{exc},y}$: Instantaneous phase of CF vortex shedding force

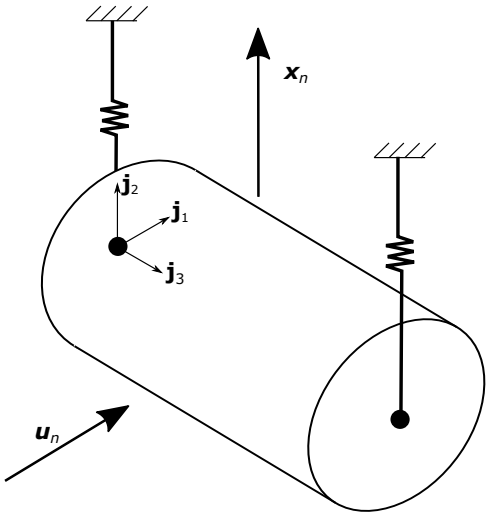

Figure 1 Spring supported model cylinder with a local coordinate system, displacement and external current velocity.

with $\boldsymbol{v}_n = \boldsymbol{u}_n - \dot{\boldsymbol{x}}_n$ being the relative flow velocity in the $\mathbf{j}_1\mathbf{j}_2$-plane. The instantaneous phase $\phi_{\text{exc},y}$ is formulated by a synchronization model, that works by adjusting the instantaneous frequency of the CF excitation force to be in phase with the velocity. In a dynamic VIV simulation, the phases are calculated in every time step by looking back in the time histories. The synchronization model is defined as:

$$\frac{d\phi_{\text{excy},y}}{dt} = \frac{2\pi|\boldsymbol{v}_n|}{D} f_{\text{exc},y}, \tag{2}$$

where the instantaneous frequency of the excitation force is:

$$f_{\text{exc},y} = \bar{f}_0 + \Delta\bar{f}\sin(\phi_{\dot{y}} - \phi_{\text{exc},y}). \tag{3}$$

The two terms, $\phi_{\dot{y}}$ and $\phi_{\text{exc},y}$ are the instantaneous phases of the cylinder velocity and the CF excitation force, respectively. The non-dimensional frequency $\bar{f}_0$ defines the center and $\Delta\bar{f}$ defines the range of the synchronization.

To summarize, the CF VIV force model has four unknown hydrodynamic parameters (C_D, C_V, $\bar{f}_0$ and $\Delta\bar{f}$) which should all be estimated. In this paper, only C_V and $\bar{f}_0$ were focused on.

3. Numerical model

The cylinder model had a diameter $D = 0.1\,\mathrm{m}$, length $L = 1\,\mathrm{m}$ and a mass of 13.05 kg, corresponding to a mass ratio of $m^* = 1.66$. The cylinder was modeled by the FEM software RIFLEX using 10 beam elements [12]. A large bending stiffness was chosen to assure a stiff cylinder. The cylinder was placed horizontally below the water surface with both ends attached to vertical springs, shown in Fig. 1. Pure CF vibrations were assured by making $\mathbf{j}_2$ the only DOF and having all other translations and rotations in the end points fixed. The spring stiffness was $598.6\,\mathrm{N/m}$ for each spring. The flow speed was set to $u = 1\,\mathrm{m/s}$ resulting in a Reynolds number of 10^5.

The external force model in Eq. 1 was applied and the non-linear dynamical equations were solved using Newmark-beta integration with $\gamma = 0.505$ and $\beta = 0.256$ and with Newton-Raphson time iteration at each time step. The time step size was $0.01\,\mathrm{s}$ and the total simulation time was set to $50\,\mathrm{s}$. For all simulations, the first 10 s were disregarded to remove transients.

4. Bayesian optimization

Bayesian optimization aims at solving the following optimization problem:

$$\hat{\boldsymbol{x}} = \arg\max_{\boldsymbol{x}\in\mathcal{A}} g(\boldsymbol{x}), \tag{4}$$

where $\boldsymbol{x} \in \mathcal{A} \subseteq \mathbb{R}^d$ is a set of hyper parameters and d is the dimension of the parameter space, typically with $d \leq 20$ [20]. The parameter space, $\mathcal{A}$, is typically a hyper-rectangle with boundaries based on prior knowledge of the parameters. This knowledge might come from earlier experience and physical limitations of the parameters. The objective function, g, is a continuous function which is typically modeled by a Gaussian process (GP). It can be a complicated function involving both data driven model-fitting and simulations which can be computationally expensive to evaluate.

The Bayesian optimization algorithm is an iterative procedure, that starts by establishing a prior distribution of g, which is usually a Gaussian process regression (GPR) with a mean and a covariance function:

$$g(\boldsymbol{x}) \sim \mathcal{GP}(\mu(\boldsymbol{x}), \Sigma(\boldsymbol{x}, \boldsymbol{x}')). \tag{5}$$

The mean is $\mu(\boldsymbol{x}) = \mathbb{E}[g(\boldsymbol{x})]$ and the covariance is $\Sigma(\boldsymbol{x}, \boldsymbol{x}') = \mathbb{E}[g(\boldsymbol{x} - \mu(\boldsymbol{x}))g(\boldsymbol{x}' - \mu(\boldsymbol{x}'))]$ with $\boldsymbol{x}$ and $\boldsymbol{x}'$ denoting two different locations in $\mathcal{A}$. It is common to use a prior with a constant mean and a covariance function which is often chosen as a squared exponential or Matérn kernel [22]. As new observations are achieved, by either new data or simulations, they are used to update the prior belief to a posterior belief. The location of the next observation in $\mathcal{A}$ is determined by the optimization of an acquisition function. Acquisition functions are normally in-expensive to evaluate and can be designed in various ways. One of the most common acquisition functions is the expected improvement (EI) which is designed to take two properties into account: *Exploration* of the areas in $\mathcal{A}$ where there is limited knowledge according to the current posterior and *exploitation* of the areas in $\mathcal{A}$ located close to the current best observation, $\boldsymbol{x}^+$. In this way the EI acquisition function reduces the chance of finding a local maximum. When g is a GP the EI acquisition function can be written as [20]:

$$\text{EI}(\boldsymbol{x}) = \delta(\boldsymbol{x})\Phi\left(\frac{\delta(\boldsymbol{x})}{\sigma(\boldsymbol{x})}\right) + \sigma(\boldsymbol{x})\phi\left(\frac{\delta(\boldsymbol{x})}{\sigma(\boldsymbol{x})}\right), \tag{6}$$

Here $\sigma(\boldsymbol{x})$ is the standard deviation of the current GP posterior prediction, $\delta(\boldsymbol{x}) = \mu(\boldsymbol{x}) - g(\boldsymbol{x}^+) - \gamma$ with $\mu(\boldsymbol{x})$ being the posterior mean, $g(\boldsymbol{x}^+)$ is the posterior mean of the current best observation and $\gamma \geq 0$ is a parameter that can be selected to provide the EI acquisition function to be more exploratory. Φ and ϕ are the standard normal CDF and PDF, respectively. The Bayesian optimization algorithm is formulated in steps given in Algorithm 1.

Algorithm 1 Bayesian optimization pseudo-code

Select a GP prior of $g(\boldsymbol{x})$
Select n_0 initial observations and compute the objective function to get $g(\boldsymbol{x}_1), ..., g(\boldsymbol{x}_{n_0})$
while No stopping criteria is met **do**
    Use the available observations to update the posterior on g with GPR
    Optimize the acquisition function to select a new point to obtain an observation
    Evaluate the objective function with the new observation, $g(\boldsymbol{x}_j)$
end while
Return the parameters associated with the best observation or the maximum posterior mean

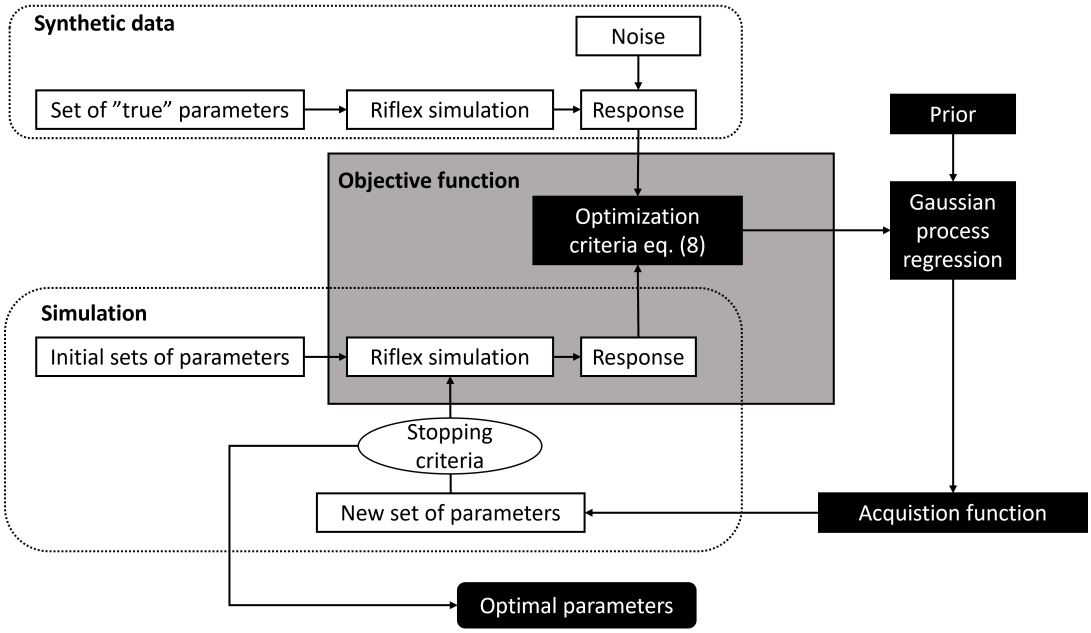

Figure 2 Optimization loop

5. VIV parameter prediction

The case study concerns the VIV parameters used in the semi-empirical force model applied for VIV time domain analysis of pure CF vibrations. The key idea of this study was to run simulations with different sets of VIV parameters, in order to find the parameter set that minimizes the response error between the simulation and the data. In this study, synthetic data was applied to illustrate the Bayesian optimization method, study its feasibility, and gain knowledge on the correlations between parameters and estimate the parameter uncertainties. The numerical model defined in Section 3. was applied in all simulations to generate synthetic data. An overview of the method for updating the parameters with Bayesian optimization is shown in Fig. 2.

5.1. Optimization algorithm

The synthetic data set was generated by selecting a parameter set and performing a time domain simulation in RIFLEX to obtain a time series of the CF displacement and corrupt it with noise. Gaussian white noise with a level of 10% was added to the signal. VIV experiments declare a measurement error for accelerometers between 1% and 2% [23]. The parameter set used for the synthetic data will be referred to as the *true parameters* denoted by and the response features from the time series are a vector $\boldsymbol{y}^{\text{data}} \in \mathbb{R}^K$ with K being the number of response features.

The objective function illustrated as the grey box in Fig. 2 takes any set of VIV parameters $\boldsymbol{x}$ as input and executes a RIFLEX simulation to get the time series of the CF response. The response features of the simulation $\boldsymbol{y}^{\text{sim}} \in \mathbb{R}^K$ and the synthetic data $\boldsymbol{y}^{\text{data}}$ are then compared. A weighted sum of the absolute relative error of the response features is used as a optimization criteria in the objective function [24]:

$$g(\boldsymbol{x}) = -\sum_{i=1}^{K} w_i \left| \frac{y_i^{\text{sim}}(\boldsymbol{x}) - y_i^{\text{data}}}{y_i^{\text{data}}} \right|. \tag{7}$$

with w_i being the weights.

The difference between the response features is formulated such that the maximum of the objective function corresponds to the minimum error between the simulation and the synthetic data. In this exam-

ple, two response features are used. The standard deviation of the non-dimensional oscillation amplitude $\sigma = \text{std}(A/D)$, with A being the CF amplitude, and the dominating oscillation frequency f. The optimization criteria from Eq. 7 become:

$$g(\boldsymbol{x}) = -w_1 \left| \frac{\sigma^{\text{sim}}(\boldsymbol{x}) - \sigma^{\text{data}}}{\sigma^{\text{data}}} \right| - w_2 \left| \frac{f^{\text{sim}}(\boldsymbol{x}) - f^{\text{data}}}{f^{\text{data}}} \right|, \tag{8}$$

where the weights w_1 and w_2 are determined such that the two terms in Eq. 8 have same orders of magnitude.

After the experiment was generated, a search space of the hydrodynamic parameters was defined. Initial simulations were performed using the parameters in the corners of the parameter space resulting in 2^d initial observations, where d is the number of parameters. The objective function was computed for the initial simulations.

The optimization process was implemented using the Bayesian optimization framework BoTorch [25] in Python. Here, a single-task GP with a fixed noise level was defined with a zero mean and a Matérn kernel with $\nu = 2.5$ and a Gamma prior length scale. Parameters were normalized to a unit cube in this framework.

The EI acquisition function in Eq. 6 with $\gamma = 0$ was maximized to obtain the parameter set $\boldsymbol{x}_n$ to be used in the next simulation. The new simulation was compared to the synthetic data by computing Eq. 8 and the posterior was updated. The optimization process stopped when the maximum posterior mean had not changed more than ϵ for m iteration steps, and the change of distance in parameter space of the parameter set associated with the maximum posterior mean did not change more than ϵ, where $\epsilon = 0.01$ and $m = 3$.

5.2. Estimating uncertainties on parameters

The uncertainty in the posterior was introduced in two ways: as model uncertainty and as data uncertainty. The model uncertainty comes from the stochastic nature of GP in Eq. 5, which was introduced through the covariance function, $\Sigma(\boldsymbol{x}, \boldsymbol{x}')$, when $\boldsymbol{x} \neq \boldsymbol{x}'$. The data uncertainty originates from the measurement error in the synthetic data and was introduced as a fixed noise level, ϵ_g, making sure that the covariance at the observed locations was $\Sigma(\boldsymbol{x}, \boldsymbol{x}' = \boldsymbol{x}) > 0$. The total posterior variance can therefore be seen as a combined data uncertainty and model uncertainty. The total uncertainty does, however, only relate to the posterior itself as an output value of the objective function, and must be transferred to an uncertainty prediction related to the parameters. Two methods to predict the uncertainty of the parameters are proposed here:

U1: The standard deviation of the $2^d + 1$ observations with the highest objective function score.

U2: A distribution of parameters associated with the best objective function scores computed from a number of GP realizations.

The uncertainty estimates depend on the selected constant noise level in the posterior. To decide the noise level, the same set of parameters was selected for both the synthetic data and the simulation, Monte Carlo sampling of the objective function was done with 100 different synthetic data responses with 10% Gaussian noise and the standard deviation was computed. A fixed noise level of $\epsilon_g = 10^{-3}$ on the posterior was found satisfactory.

6. Results for 1 DOF system

The values $C_D = 1.2$ and $\Delta\bar{f} = 0.64$ were selected for all cases. The true parameters for the synthetic data were $C_V = 0.85$ and $\bar{f}_0 = 0.144$. All parameters were selected based on earlier studies in [15]. The boundaries for C_V were [0.2, 1.3] and for $\bar{f}_0$ were [0.09, 0.2].

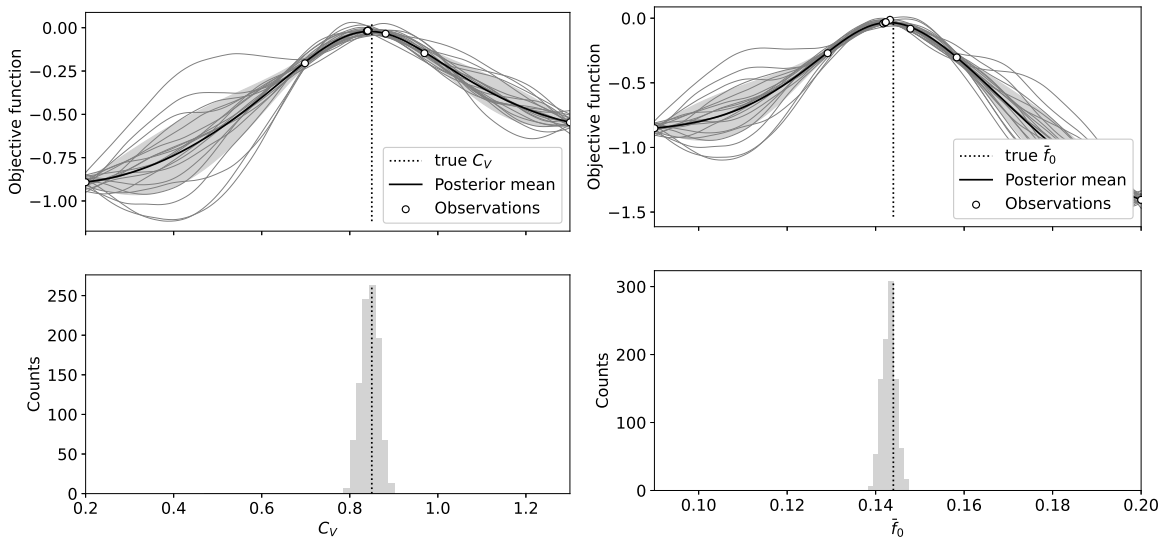

(a) (b)

Figure 3 Posterior mean and posterior standard deviation bounds for optimizing single parameters, C_V in (a) and $\bar{f}_0$ in (b). The thin grey lines illustrate individual GP realizations drawn from the posterior. The histograms show the distributions of individual maxima from 1000 GP realizations.

6.1. Single parameter optimization

A single parameter was tuned while the other was assumed to be deterministic by setting it to the true value. Two initial simulations were executed with the parameter values at the lower and upper boundary. The objective function in Eq. 8 was applied with the weights $w_1 = 1$ and $w_2 = 5$. The value for w_2 was selected according to the amplitude criteria in Eq. 8 which in general was more than a factor of 5 larger than the frequency criteria. The optimal values for the weights will need further studies.

A solution of the optimization problem in Eq. 4 was found with the Bayesian updating method explained in Section 5.. The final posterior mean and the standard deviations are shown in Fig. 3 along with the two initial observations and the additional observations gathered in the optimization process. The grey lines illustrate GP realizations drawn from the posterior distribution. The individual maximum of 1000 of GP realizations were computed, and the parameter values associated with the maxima were presented in the histograms. Convergence to the true value is seen in all cases after 3 to 4 additional observations.

6.2. Dual parameter optimization

Two parameters, C_V and $\bar{f}_0$, were tuned simultaneously. The initial observations were computed in the corners of the parameter space, and Bayesian optimization was used to select additional observations as shown in Fig. 4. The best observation was seen to converge to the true parameters after 9 additional observations in Fig. 5(a). In the same figure, the error estimates at each iteration step are shown to illustrate how the parameter uncertainty decrease and stabilizes as more observations are obtained. The distributions of the individual posterior maxima made from 1000 GP realizations of the last iteration step are shown in Fig. 5(b). The histograms and uncertainty estimates for the dual-parameter study were computed similarly to the single-parameter study, so the correlation effect and joint distributions were not considered. It should be noted that only a weak correlation is seen between C_V and $\bar{f}_0$ which is resulting in a quick and precise prediction of the posterior maximum. In cases where the parameters are strongly correlated the algorithm might take longer to converge or might end up in a local maximum instead. In Table 1, the predicted parameters of the last iteration are shown for both single-parameter

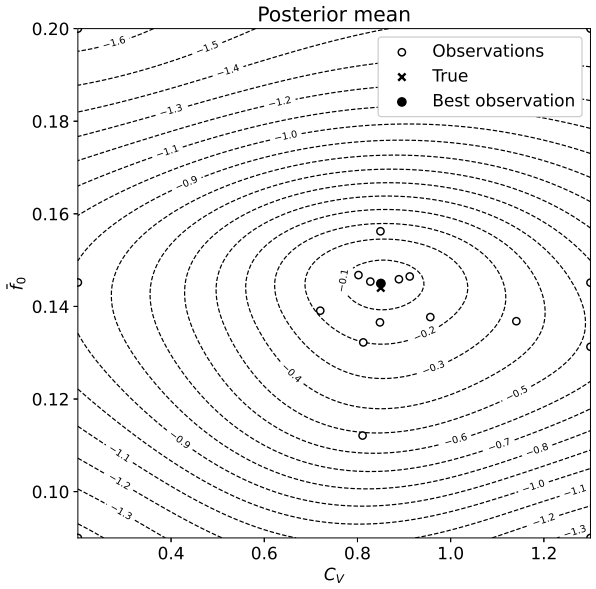

Figure 4 Posterior mean surface contour for C_V and $\bar{f}_0$ including all observations.

Table 1 Predicted values for C_V and $\bar{f}_0$ and the estimated uncertainties using the two methods explained in Subsection 5.2..

	Single parameter optimization		Dual parameter optimization	
Uncertainty method	C_V	$\bar{f}_0$	C_V	$\bar{f}_0$
U1	0.845 ± 0.001	0.143 ± 0.001	0.854 ± 0.045	0.145 ± 0.003
U2	0.845 ± 0.025	0.143 ± 0.002	0.854 ± 0.038	0.145 ± 0.005

optimizations and the dual-parameter optimization. The predicted parameters show good agreement with the true values and both uncertainty prediction methods demonstrate small parameter uncertainty. When the parameters were estimated alone, the uncertainties were smaller than when both parameters were estimated simultaneously. For the single parameter optimization, U1 results in a lower uncertainty than U2, This is not the case for the dual parameter optimization, where U1 results in a higher uncertainty for C_V and a lower uncertainty for $\bar{f}_0$ than U2. A drawback of both uncertainty estimation methods is that they both depend on the choice of objective function in Eq. 8. Using other terms than σ and f, including more terms, changing the weights or replacing the absolute errors with squared errors will have an impact on how well the uncertainties are estimated.

7. Concluding remarks

In this paper, a Bayesian optimization framework was applied to tune two of the hydrodynamic parameters in a simplified time-domain VIV model for CF vibrations only. VIV on a rigid cylinder model was used for the purpose of illustrating the method and synthetic data was generated from the time-domain model itself. An objective function was defined to run a simulation using a set of hydrodynamic parameters and return a response error. A weighted sum of absolute errors included both response in CF amplitude and frequency. The following results were obtained from the study:

- The additional observations needed to estimate true parameters were less than 4 for the single parameter optimization and less than 9 for the dual parameter optimization.

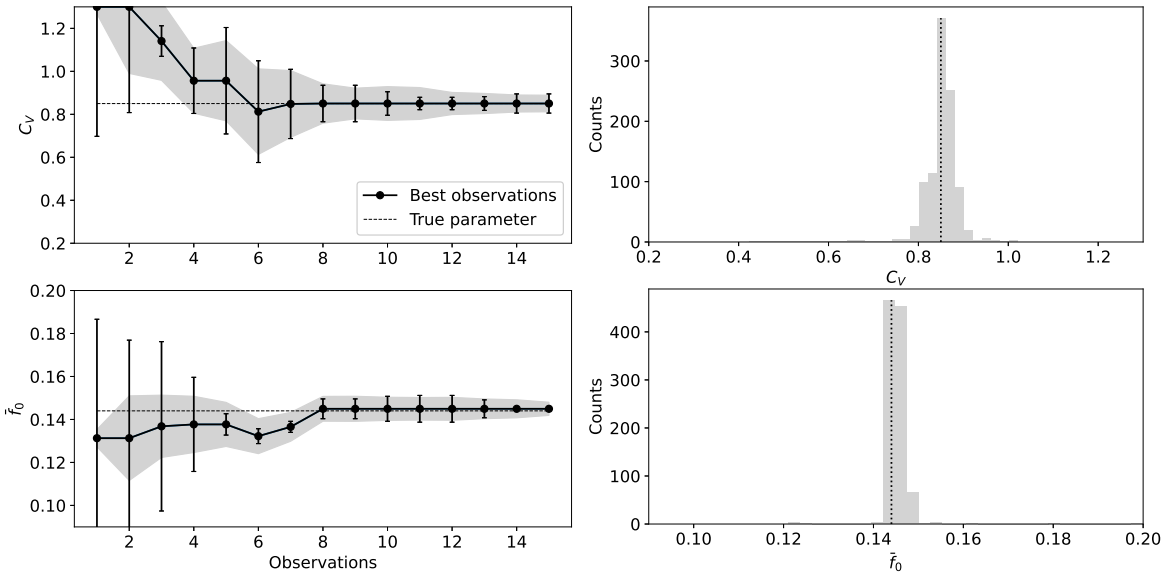

(a) (b)

Figure 5 (a) Convergence of the best observation as new observations (in addition to the initial observations) are introduced. The error bars represent the std of the best 5 observations and the grey band is the standard deviation of 1000 GP realization maxima. (b) Uncertainty histograms made from the individual maxima of 1000 GP realizations from the final posterior.

- Two methods to estimate the parameter uncertainty were introduced: U1 that applies the additional observations and U2 that applies a distribution of maxima from individual GP realizations.
- U1 and U2 both reduced the parameter uncertainty as more observations were included.

The study showed that the optimization method is feasible for 1 DOF using a simplified VIV model and simulated data. The plan for further extension of the research involves data from model tests with both CF and IL vibrations, an examination of different objective functions and uncertainty methods. A sensitivity analysis will be performed to select parameters that has the greatest influence on amplitude and frequency in the optimization process.

Acknowledgements

The authors wish to thank everyone involved in the PRAI project and are especially thankful for the collaboration with Dr. Sølve Eidnes and Dr. Kjetil Olsen Lye from SINTEF Digital. We would also like to thank the Norwegian Research Council, Equinor, BP, Kongsberg Maritime, Subsea7 and Aker Solutions for supporting the PRAI project.

References

[1] Turgut Sarpkaya. A critical review of the intrinsic nature of vortex-induced vibrations. *Journal of fluids and structures*, 19(4):389–447, 2004.

[2] B Mutlu Sumer and Jørgen Fredsøe. *Hydrodynamics Around Cylindrical Structures*. WORLD SCIENTIFIC, revised edition, 2006.

[3] DNVGL. *Recommended practice DNV-RP-F204 - Riser fatigue*, 2010.

[4] Ramnarayan Gopalkrishnan. Vortex-induced forces on oscillating bluff cylinders. Technical report, Woods Hole Oceanographic Institution MA, 1993.

[5] J Kim Vandiver and Li Li. Shear7 v4. 4 program theoretical manual. *Massachusetts Institute of Technology*, 2005.

[6] Michael Triantafyllou, George Triantafyllou, YS Tein, and Bill D Ambrose. Pragmatic riser viv analysis. In *Offshore technology conference*. OnePetro, 1999.

[7] Carl M Larsen, Kyrre Vikestad, Rune Yttervik, Elizabeth Passano, and GS Baarholm. Vivana theory manual. *Marintek, Trondheim, Norway*, 2001.

[8] M.J. Thorsen, S. Sævik, and C.M. Larsen. A simplified method for time domain simulation of cross-flow vortex-induced vibrations. *Journal of Fluids and Structures*, 49:135–148, 2014.

[9] Jan Vidar Ulveseter, Svein Sævik, and Carl Martin Larsen. Time domain model for calculation of pure in-line vortex-induced vibrations. *Journal of Fluids and Structures*, 68:158–173, 2017.

[10] M.J. Thorsen, S. Sævik, and C.M. Larsen. Fatigue damage from time domain simulation of combined in-line and cross-flow vortex-induced vibrations. *Marine Structures*, 41:200–222, 2015.

[11] Eugene M Izhikevich, Yoshiki Kuramoto, et al. Weakly coupled oscillators. *Encyclopedia of mathematical physics*, 5:448, 2006.

[12] SINTEF Ocean. *RIFLEX 4.15.0 Theory Manual*, 2018.

[13] E Passano, J Wu, Sævik S., and D. Yin. *VIVANA-TD Theory/User manual*. SINTEF Ocean, Trondheim, Norway, 2020.

[14] J.V. Ulveseter, M.J. Thorsen, S. Sævik, and C.M. Larsen. Simulating fundamental and higher harmonic viv of slender structures. *Applied Ocean Research*, 90:101856, 2019.

[15] Sang Woo Kim, Svein Sævik, Jie Wu, and Bernt Johan Leira. Prediction of deepwater riser viv with an improved time domain model including non-linear structural behavior. *Ocean Engineering*, 236:109508, 2021.

[16] Sang Woo Kim, Svein Sævik, Jie Wu, and Bernt Johan Leira. Simulating high-mode vortex-induced vibration of a riser in linearly sheared current using an empirical time-domain model. *Journal of Offshore Mechanics and Arctic Engineering*, 143(4):041901, 2021.

[17] Decao Yin, Jie Wu, Halvor Lie, Jingzhe Jin, Elizabeth Passano, Svein Saevik, Signe Riemer-Sorenson, Anne Marthine Rustad, Michael A Tognarelli, Guttorm Grytyr, et al. Optimization of hydrodynamic coefficients for viv prediction. In *International Conference on Offshore Mechanics and Arctic Engineering*, volume 85185, page V008T08A025. American Society of Mechanical Engineers, 2021.

[18] Xu Han, Bernt Johan Leira, and Svein Sævik. Vessel hydrodynamic model tuning by discrete bayesian updating using simulated onboard sensor data. *Ocean Engineering*, 220:108407, 2021.

[19] Xuhui Meng, Zhicheng Wang, Dixia Fan, Michael S Triantafyllou, and George Em Karniadakis. A fast multi-fidelity method with uncertainty quantification for complex data correlations: Application to vortex-induced vibrations of marine risers. *Computer Methods in Applied Mechanics and Engineering*, 386:114212, 2021.

[20] Peter I Frazier. A tutorial on bayesian optimization. *arXiv preprint arXiv:1807.02811*, 2018.

[21] Raul Astudillo and Peter I Frazier. Thinking inside the box: A tutorial on grey-box bayesian optimization. In *2021 Winter Simulation Conference (WSC)*, pages 1–15. IEEE, 2021.

[22] Carl Edward Rasmussen. Gaussian processes in machine learning. In *Summer school on machine learning*, pages 82–89. Springer, 2003.

[23] A.D. Trim, H. Braaten, H. Lie, and M.A. Tognarelli. Experimental investigation of vortex-induced vibration of long marine risers. *Journal of Fluids and Structures*, 21(3):335–361, 2005. Marine and Aeronautical Fluid-Structure Interactions.

[24] Tinkle Chugh. Scalarizing functions in bayesian multiobjective optimization. In *2020 IEEE Congress on Evolutionary Computation (CEC)*, pages 1–8. IEEE, 2020.

[25] Maximilian Balandat, Brian Karrer, Daniel R. Jiang, Samuel Daulton, Benjamin Letham, Andrew Gordon Wilson, and Eytan Bakshy. BoTorch: A Framework for Efficient Monte-Carlo Bayesian Optimization. In *Advances in Neural Information Processing Systems 33*, 2020.